

Long-range ordering of Sb multilayers on GaAs(110): Evolution of resonant inverse photoemission

Yongjun Hu, M. B. Jost, T. J. Wagener, and J. H. Weaver

Department of Materials Science and Chemical Engineering, University of Minnesota, Minneapolis, Minnesota 55455

(Received 29 May 1990)

Temperature- and coverage-dependent ordering of Sb multilayers on GaAs(110) has been investigated with use of inverse-photoemission spectroscopy (IPES) and low-energy electron diffraction. IPES studies show that an empty state at $E_F + 0.3$ eV resonates for incident electron energies of $E_i = 16.2$ eV because the radiative decay of a plasmon within the Sb film ($\hbar\omega_p = 15.9$ eV) competes with conventional inverse photoemission. The resonance is first observed at ~ 3.5 monolayers (ML) as the empty-state feature shifts from ~ 0.4 eV at 3 ML to ~ 0.3 eV at 3.5 ML for Sb overlayers grown on GaAs(110) at 300 K and annealed to 475 K. The empty structure is associated with long-range ordering of the Sb multilayers rather than Sb-As antibonding states at the interface. The thin film structure and the thickness of the film play critical roles in determining the empty-state resonance. Structural studies for 20-Å Sb films show ringlike diffraction patterns with the coexistence of (1×1) structures and fractional-order spots adjacent to integer-order spots along $[11]$ or $[1\bar{1}]$. The ringlike structures are attributed to hexagonal basal planes of individual Sb crystallites that are randomly rotated and oriented parallel to the (110) surface. Two equivalent quasihexagonal domains are observed during the initial growth stages. These results suggest a correlation between the resonance and growth phases consisting of long-range-ordered (110) domains with Sb crystallites in between.

INTRODUCTION

Surface long-range ordering and the flattening of semiconducting or metallic thin films on semiconductor substrates have been the subject of experimental and theoretical studies for many years.¹ In particular, Sb thin-film growth on GaAs(110) has attracted attention because it provides a nondisruptive, epitaxial-overlayer-semiconductor interface system.²⁻¹⁴ Photoemission (PES), Auger-electron spectroscopy, low-energy electron diffraction (LEED), and thermal-desorption spectroscopy (TDS) studies have revealed modified Stranski-Krastanov, or monolayer-plus-multilayer simultaneous growth for Sb deposition at ~ 300 K.²⁻⁸ Deposition of 1 monolayer (ML) of Sb at 300 K produces a nearly perfect (1×1) ordered overlayer, although some local disorder may persist.⁷ For coverages greater than 1 ML, 300-K deposition results in the growth of three-dimensional islands atop the initial Sb monolayer without long-range order.^{3,4} Moreover, the surface morphology depends on annealing temperatures and film thicknesses. Carelli and Kahn³ have shown that the desorption of Sb adatoms in excess of 1 ML occurs for annealing temperatures greater than ~ 525 K, and that the resulting ordered 1 ML Sb overlayer was stable to 825 K.

Most previous studies have concentrated on the initial growth stages of the (1 ML Sb)/GaAs(110) interface. Very few have correlated the evolution of the surface morphology with changes in the electronic structure of multilayer films. In an interesting paper, however, Drube and Himpfel¹⁵ reported that a metastable 20-Å Sb film on InP(110) exhibits a very strong resonant inverse-photoemission structure at a constant photon energy of $\hbar\omega_p = 16.4$ eV that corresponds to the thin-film plasmon

energy of Sb. This resonant behavior disappeared for the stable, bulklike Sb phase.¹⁵ The resonance phenomenon is still not well understood since a minimum in the inverse-photoelectron emission is expected based on the surface-matching condition that the real part of the bulk dielectric function is equal to zero at $\hbar\omega_p$.¹⁶

This paper focuses on the evolution of the resonant structure during the growth of Sb overlayers on GaAs(110). We have performed inverse-photoemission spectroscopy (IPES) and LEED to examine the role of annealing temperature and critical thickness on the long-range ordering and flattening of Sb clusters or islands. The variation of the unique metastable structures for Sb thin films have been investigated. We show that the interaction of the various phases in this overlayer structure provides novel matching for the thin-film dielectric function at the surface, and this matching facilitates radiative plasmon decay. With these results, it is possible to correlate modifications in the structure of the Sb multilayers on GaAs(110) with the evolving empty electronic states.

EXPERIMENTAL TECHNIQUES

The experiments were carried out in a spectrometer optimized for IPES studies at photon energies of $10 \leq h\nu \leq 44$ eV.¹⁷ A highly collimated monoenergetic electron beam was directed at normal incidence onto the sample surface from an electron gun with a $1 \text{ mm} \times 5 \text{ mm}$ planar BaO cathode and Pierce-type geometry. Emitted photons dispersed by an $f/3.5$ grating monochromator were detected with a position-sensitive detector. The combined energy resolution (electrons and photons) was 0.4 eV for incident electron energies E_i of ~ 15 eV. Parallel LEED studies made it possible to correlate

changes in the electronic states with changes in surface structure. GaAs(110) surfaces (*p* type with Zn doping at $2 \times 10^{18} \text{ cm}^{-3}$) were obtained by cleaving *in situ*. The sample temperature was calibrated using a Chromel-Alumel thermocouple. Antimony was evaporated at pressures of $\sim 3 \times 10^{-10}$ Torr (experimental system base pressure $\sim 8 \times 10^{-11}$ Torr). The amount of material deposited was determined with a quartz-crystal oscillator adjacent to the sample. For this system, 1 ML of the (1 \times 1) structure corresponds to $\Theta = 2.7 \text{ \AA}$, or 8.85×10^{14} atoms/cm².

RESULTS AND DISCUSSION

Long-range ordering and resonant IPES for (20 \AA Sb)/[*p*-type GaAs(110)]

Photon-distribution curves (PDC's) for normal-incidence inverse photoemission are shown in Fig. 1 for 20 \AA Sb on *p*-type GaAs(110) measured with $E_i = 18 \text{ eV}$. The spectra have been normalized to electron dose and the throughput of the optical system,¹⁷ and energies have been referenced to the sample Fermi level E_F . Annealing temperatures and times are given alongside each PDC. The main empty electronic-state features appear at $\sim 2.25, 3.3, 5.1,$ and 6 eV above E_F for the clean GaAs(110) surface, consistent with previous IPES results.¹⁸ For 20 \AA of Sb deposited at 300 K, the weak emission at E_F indicates that the thin film is semimetallic due to the monolayer-plus-multilayer simultaneous growth of three-dimensional (3D) clusters.⁴ Poorly resolved features near 0.9, 1.8, 3.1, 4.1, and 6.1 eV can be associated with this 3D-cluster growth without long-range order.^{3,4} No LEED patterns could be seen, except for nonuniform, cloudlike structures for E_i ranging from 20 to 200 eV. This may indicate that some local, short-range order exists.

Annealing the 20 \AA Sb film at 475 K gives a very interesting LEED pattern, as shown in the middle of Fig. 1 (the LEED pattern was acquired with $E_i = 40 \text{ eV}$). The (1 \times 1) structure (open circles) persists and fractional-order spots (triangles) appear adjacent to the integer-order spots (open circles). By varying the incident LEED energy, we found that the fractional-order spots correspond to diffraction from planes parallel to (110). Compared with LEED patterns of (2 ML Bi)/GaAs(110), which show diamondlike fractional-order spots adjacent to integer-order spots,^{19,20} these extra spots sit slightly off the [11] and $[1\bar{1}]$ directions. Some of the fractional-order spots, including those outside (01) and (0 $\bar{1}$) or the ones inside (10) and ($1\bar{0}$), are missing, so that the rest seem to be mirror-symmetric relative to the [001] or $[1\bar{1}0]$ directions. This makes it difficult to interpret the details of the surface structures. In general, however, the occurrence of fractional-order spots adjacent to (110) integer-order spots can be attributed to growth of (110) domains that have been observed by scanning tunneling microscopy (STM) for Bi overlayers on GaAs(110) up to $\sim 10 \text{ ML}$.²¹ Assuming that partial long-range (110) ordering also occurs for Sb patches or islands upon annealing, it is likely that more than one of the (110) domains might be

formed because of two inequivalent sites on the initial monolayer, namely Sb(Ga) or Sb(As) sites. This is reasonable since Sb gives a better lattice match than Bi, as will be discussed later. Extinction between various domains, such as antiphase conditions and various locations of domains, might be the cause for missing some of the fractional-order spots (assuming domain sizes that are smaller than the coherence length of LEED, which is usually around a few hundred angstroms²²).

The ring structure diffraction of Fig. 1 occurs with the (00) specular beam (we show the first-order ring in Fig. 1), indicating that a large number of rotational Sb domains are formed with basal planes parallel to the (110) substrate. The ratio of radii of the first-, second-, and third-order diffraction rings is 1:1.732:2, indicating that the

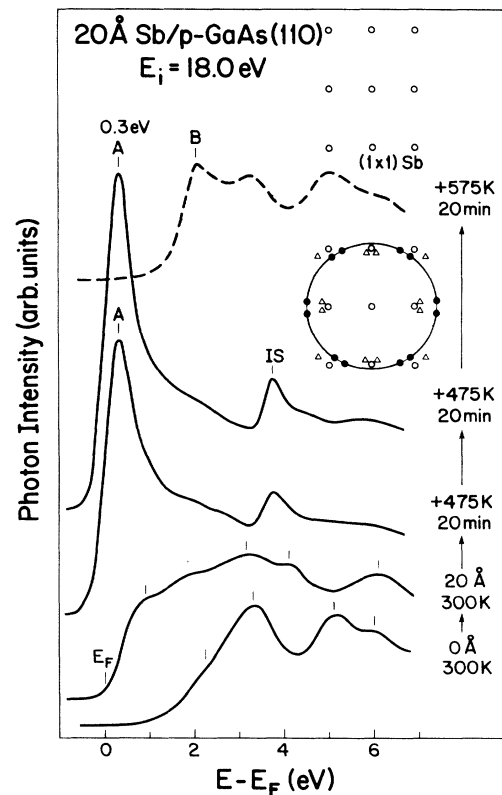


FIG. 1. Normal-incidence IPES spectra for cleaved *p*-type GaAs(110) and for (20 \AA Sb)/GaAs(110) with $E_i = 18 \text{ eV}$. The overlayer spectra were acquired after deposition at 300 K, after annealing at 475 K for 20 and 40 min, and finally after annealing at 575 K for 20 min. Feature *A* is associated with long-range order in the Sb multilayers on GaAs(110) and feature *B* is associated with a surface-resonant state largely derived from Sb-Sb $p_z - p_z \pi^*$ chain bonds for $p(1 \times 1)\text{-Sb}(1 \text{ ML})$. IS denotes an image-potential state. The top inset shows (1 \times 1) LEED patterns for $E_i = 40 \text{ eV}$ that correspond to the topmost IPES spectrum and the clean (110) surface. The middle inset schematically shows the LEED pattern for overlayers annealing at 475 K. Open circles represent integer-order spots, triangles represent fractional-order spots, and solid circles represent six-pair modulation spots observed on the ringlike structure. The centers of the six-pair spots make a hexagon.

ring structure corresponds to hexagonal-like domains. The nearest-neighbor distance is $\sim 3.74 \text{ \AA}$ for the (0001) plane, as determined from the radius of the first-order ring. This value is smaller than that of bulk Sb(001), namely 4.02 \AA ,²³ implying that the a and b axes are constrained for these Sb domains. As can be seen, the intensity of the ring structure is not uniform. Six pairs of modulation spots (solid circles) appear on the ring structure, and the centers of each pair define a hexagon. These modulation spots originate from two inequivalent quasi-hexagonal (half-hexagon) domains that form during the initial growth stage ($\sim 3.5 \text{ ML}$), as will be discussed shortly.

The IPES results of Fig. 1 show a sharp feature at 0.30 eV with a pronounced leading edge at E_F when the film is annealed at 475 K , in sharp contrast to the IPES spectrum taken after 300 K deposition. A second feature at $\sim 3.75 \text{ eV}$ develops, and it is attributed to an image-potential state (IS), as for semimetallic Bi overlayers.^{19,20} The appearance of this pronounced IS also indicates that annealing leads to a flattening of the Sb clusters. Very recently, Busch and Henzler¹ have developed spot-profile analysis of LEED to investigate flattening and ordering kinetics for overlayers on semiconductor surfaces upon annealing. They have found that the average ordered domain size increases with annealing time, and it lasts at least for a finite period at the appropriate temperature. Similar trends have been found for Sb/GaAs(110). (We will return to the issue of flattening.) Since the semimetallic Sb overlayers are quite flat, the long-range image potential can be readily seen.²² This IS contains a series of Rydberg states²² that cannot be resolved with the $\sim 0.4 \text{ eV}$ resolution of this study. The intensity of feature A near E_F gradually increases with longer annealing at 475 K , saturating after $\sim 40 \text{ min}$ as the Sb-overlayer structure stabilizes (also see Fig. 1). Note that no significant changes in the LEED or IPES results could be seen when the sample was cooled to 300 K after annealing.

According to previous studies,^{3,7} Sb adatoms in excess of 1 ML desorb from the surface upon annealing at temperature $T \geq 515 \text{ K}$. The remaining 1 ML (1×1) Sb overlayers remain stable to higher temperature (~ 600 and $\sim 825 \text{ K}$, according to Ludeke *et al.*⁷ and Kahn *et al.*³). Indeed, we found that Sb desorption occurred above 515 K for $\Theta > 1 \text{ ML}$. The topmost PDC of Fig. 1 was obtained after annealing at $\sim 575 \text{ K}$ for 20 min , and a sharp (1×1) LEED pattern was observed. The spectrum is identical to that taken from 1 ML (1×1) Sb.²⁴ Feature B at 2 eV is ascribed to an Sb-derived surface-resonant state containing Sb p_z character.²⁴

The IPES spectrum for 20 \AA Sb annealed at 475 K exhibits a pronounced resonance for feature A at 0.30 eV , as mentioned above. This is highlighted in Fig. 2 through energy-dependent IPES spectra that are plotted so that constant-photon-energy features are aligned and E_F moves from right to left with increasing incident-energy E_i . The spectra are normalized according to electron dose and the spectral throughput of the optical system.¹⁷ As can be seen, enhancement of feature A , a Sb-derived state, occurs around a constant energy $\hbar\omega_p = 15.9 \text{ eV}$, corresponding to the Sb thin-film plasmon energy re-

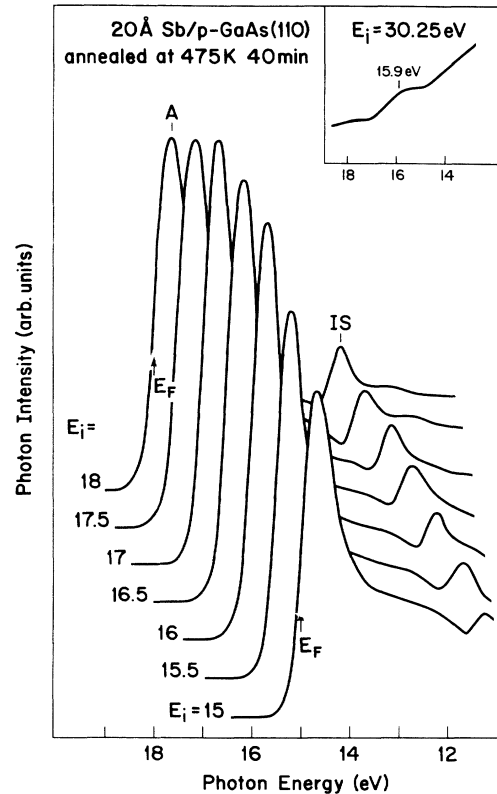


FIG. 2. Energy-dependent IPES spectra for (20 \AA Sb)/GaAs(110) after annealing at 475 K for 40 min following deposition at 300 K . The incident energy E_i is given alongside each spectrum, so that E_F moves with increasing E_i . IS denotes an image-potential state. Sb-derived feature A is resonantly enhanced around the constant photon energy $\hbar\omega_p = 15.9 \text{ eV}$, corresponding to the Sb thin-film plasmon energy. The inset shows a constant-photon-energy emission feature at $\hbar\omega_p = 15.9 \text{ eV}$ for $E_i = 30.25 \text{ eV}$.

ported in earlier IPES and electron-energy-loss-spectroscopy (EELS) studies.^{4,20} As shown in the inset of Fig. 2, the plasmon radiative decay, a constant-photon-energy emission feature, appears at $\hbar\omega_p \approx 15.9 \text{ eV}$ for $E_i = 30.25 \text{ eV}$. It does not depend on the incident-electron energy as long as $E_i > \hbar\omega_p$. This resonance is very similar to what occurs at $\hbar\omega_p = 16.4 \text{ eV}$ for (20 \AA Sb)/InP(110).¹⁵ The latter overlayer exhibits a metastable structure with extra LEED spots forming a rectangle along $[001]$ only. The interpretation for this plasmon-related resonance remains controversial.^{15,16,20} For most free-electron-like solids, a minimum in the emission intensity is found at the plasmon energy because the real part of the bulk dielectric function is equal to zero at $\hbar\omega_p$, and this gives rise to a minimum of the photon-emission probability derived from the surface-matching conditions between the radiative and initial excited plasmon fluxes.¹⁶

Empty electronic-state evolution with Sb desorption for (20 \AA Sb)/[p -type GaAs(110)]

To gain insight into the evolution of the structure-dependent electronic states of Sb overlayers, we varied

the thickness of Sb overlayers by using annealing and cooling steps between the desorption temperature (~ 515 – 540 K for Sb adatoms in excess of 1 ML) and 300 K. The predesorption results were identical to those in Fig. 2. Figure 3 shows representative results for (20 Å Sb)/[*p*-type GaAs(110)] for $E_i = 16.5$ eV, where feature *A* can be seen to decrease after annealing at ~ 515 K for 20 min. A new Sb-derived state, feature *B*, appears at ~ 2 eV and then increases, while feature *A* decreases with annealing at $T \geq 515$ K. Concurrently, LEED shows that the intensity of the ring structure gradually diminishes with the annealing (the ring intensity reduced faster than the six pairs of modulation spots).

As shown in Fig. 3, feature *A* is smaller than feature *B* after annealing at ~ 535 K for 10 min. LEED shows that the ring structure and its modulation spots have almost disappeared under these conditions, but the fractional-order spots near integer-order spots persist. After annealing at ~ 545 K for 20 min, the LEED pattern shows only a sharp (1×1) structure, and the IPES spectrum shown in Fig. 3 is identical to that for 1 ML (1×1) Sb on *p*-type GaAs(110).²⁴ As demonstrated by Drube *et al.*,²⁴ 1 ML (1×1) Sb overlayers are semiconducting with a band offset of ~ 1 eV and a surface-resonant state at ~ 2 eV above E_F . Differences in IPES spectra for $E_i = 16.5$ and 18 eV in Figs. 1 and 3 are due to band-structure effects, i.e., momentum dependence. A should-

er at ~ 3.2 eV has been attributed to a GaAs bulk state that is not affected by Sb adatoms.²⁴

Long-range ordering and overlayer flattening for (2 ML Sb)/[*p*-type GaAs (110)]

To better understand the origins of Sb-derived features *A* and *B*, we investigated their evolution as a function of the temperature. Figure 4 shows the effects of annealing for (2 ML Sb)/[*p*-type GaAs(110)] with $E_i = 16.5$ eV (2 ML = 5.4 Å). The LEED results show a sharp (1×1) pattern with weakly increasing background after deposition at 300 K, consistent with Sb-cluster growth without long-range order atop the initial (1×1) ordered monolayer.^{3,4} From the IPES spectrum of Fig. 4, the conduction-band offset is ~ 0.3 eV above E_F , indicating that 2 ML Sb grown at 300 K is semiconducting. The Sb-derived state at $E_F + 1.85$ eV is probably associated with the first ordered monolayer of Sb. Features at ~ 2.9 and 4.5 eV may be related to high-coverage, bulklike Sb states and GaAs bulk bands in uncovered areas. The weak shoulder at ~ 1 eV may be attributed to Sb—Sb bonds in Sb clusters without long-range order.

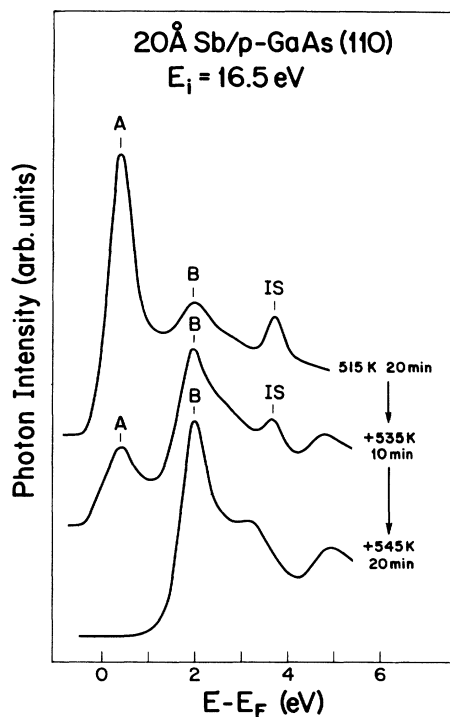


FIG. 3. Evolution of empty electronic states during thermal desorption of (20 Å Sb)/GaAs(110). The predesorption spectrum is identical to that of Fig. 2, and the bottommost curve is identical to that for (1×1)-Sb(1 ML). During desorption, feature *B* increased while feature *A* decreased. IS denotes an image-potential state.

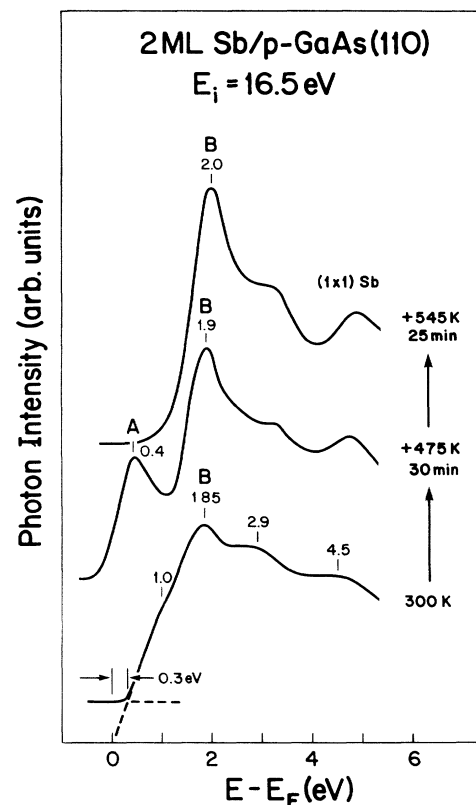


FIG. 4. Empty-electronic-state evolution during long-range ordering of 2 ML Sb on GaAs(110). The IPES spectra were acquired after 300 K deposition with annealing cycles as shown. Feature *A* appears at $E_F + 0.40$ eV after annealing at 475 K. Further annealing at 545 K resulted in an increase of feature *B* and the disappearance of feature *A* due to the Sb desorption. The topmost curve is identical to that for (1×1)-Sb(1 ML). Parallel structural changes are discussed in the text.

The clusters grown by 2 ML deposition are not large enough to form metallic (semimetallic) layers (~ 3 ML Sb is required to form a discernible Fermi edge at 300 K). Upon annealing at 475 K for 30 min, however, two sharp features, *A* and *B*, appear at 0.4 and 1.9 eV, respectively, and a sharp Fermi edge develops (Fig. 4). This spectrum is very similar to the middle PDC of Fig. 3, although the intensity of feature *A* is weaker and a less-pronounced image-potential state still persists in Fig. 3. LEED gives identical structures, namely fractional-order spots adjacent to integer-order spots nearly along $[11]$ or $[\bar{1}\bar{1}]$. No ring structures or hexagonlike modulation spots can be found. This demonstrates that long-range-ordered Sb patches or islands have been flattened out on the initial Sb overlayers upon annealing at an intermediate temperature of ~ 475 K. The Sb-Sb interaction arising from these ordered multilayers changes the electronic properties of this Sb thin film and results in a transition from a semiconducting to a metallic film. After further annealing at the desorbing temperature of ~ 545 K for ~ 25 min, LEED again shows a sharp (1×1) structure only. The corresponding IPES spectrum (top PDC of Fig. 4) is indistinguishable from the bottommost curve for the (1×1) Sb(1 ML) of Fig. 3. The movement of feature *B* from 1.9 to 2.0 eV above E_F in Fig. 4 can be associated with band-bending changes (usually ~ 100 meV) between 1 and 2 ML Sb on *p*-type GaAs(110).^{7,13}

Critical thicknesses and resonant IPES

Feature *A* at $E_F + 0.40$ eV is associated with long-range ordering or flattening of Sb atop the initial monolayer, as discussed above (Fig. 4). Interestingly, there is no resonant enhancement of feature *A* at $\hbar\omega_p = 15.9$ eV for (2 ML Sb)/GaAs(110), based on energy-dependent studies analogous to those described above for 20 Å films (Fig. 2). Hence, it is important to determine the critical thickness at which the phenomenon first appears.

In Fig. 5 we show coverage-dependent IPES spectra taken after 300 K deposition and after annealing at 475 K for 20 min for representative coverages of 3, 3.5, and 4 ML. Weak emission appears at E_F for 300 K deposition of 3 ML Sb. This indicates that some of the as-grown clusters are semimetallic. Feature *B* at 1.85 eV, associated with the ordered first monolayer, is much weaker than for the 2 ML case (Fig. 4) because of increasing cluster-size effects. Other features are poorly resolved because the Sb clusters have no long-range order.^{3,4} For 3 and 4 ML films grown at 300 K, the emission remains quite weak at E_F , no significant feature *A* can be seen, and feature *B* gradually fades. For $\Theta = 3.5$ ML, a weak shoulder does appear at ~ 0.75 eV, and it is more pronounced at ~ 1.0 eV for $\Theta = 4$ ML. A weak image-potential state feature also appears at ~ 4 eV for 4 ML, revealing that some extended patches have become semimetallic (large flat metallic planes exhibit a sharp IS).¹⁹ Overall, the spectra for 300 K deposition are relatively structureless. LEED shows that the (1×1) structure gradually disappears and the background increases, but no new spots appear.

Annealing at 475 K for 20 min produces ordered sur-

face structures. For $\Theta = 3$ ML, the (1×1) LEED structure, the fractional-order spots look identical to those of 2 ML, and the intensities of the fractional-order spots become much stronger. For $\Theta = 3.5$ ML, in addition to the

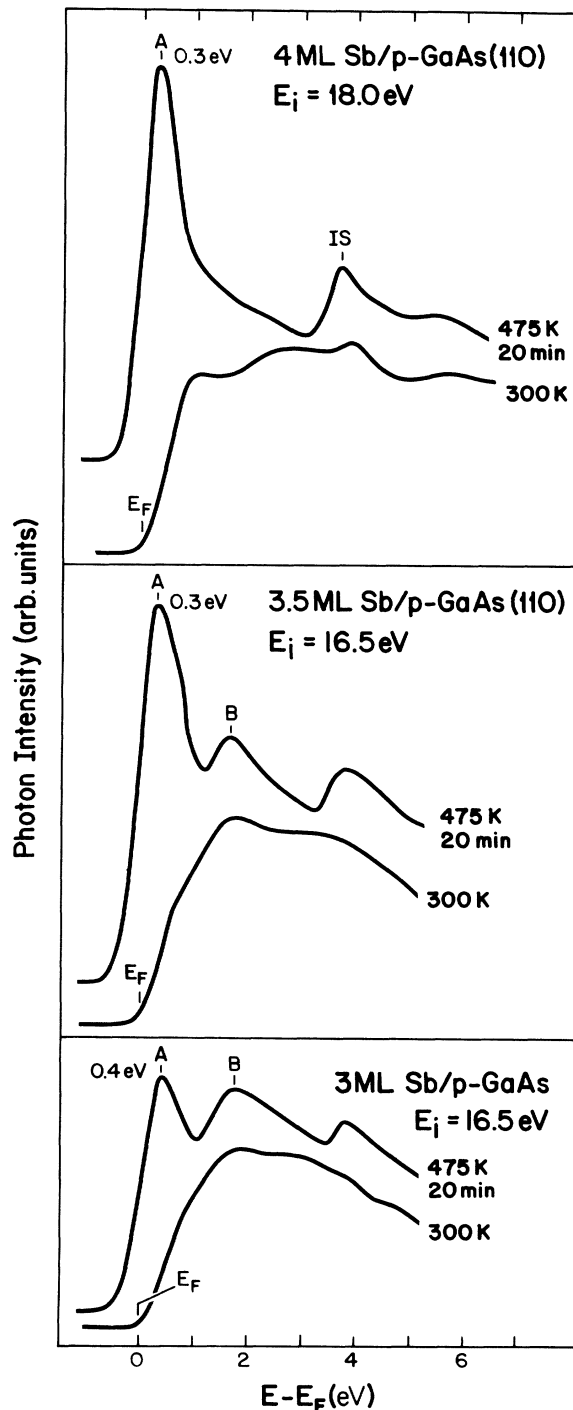


FIG. 5. Effects of coverage-dependent long-range ordering. The IPES spectra were acquired after deposition at 300 K and after annealing at 475 K for 20 min. Feature *B* is suppressed at 4 ML, and feature *A* shifts from 0.40 eV at 3 ML to 0.30 eV at 3.5 ML upon annealing and ordering. IS denotes an image-potential state.

(1×1) structure and the fractional-order spots observed at 3 ML, some of the six-pair modulation spots on the ring structure shown in Fig. 1 become barely visible, even though the ring structure cannot be identified. For $\Theta=4$ ML the six-pair modulation spots can be clearly identified, but the ring structure is still hardly discernible.

The IPES results of Fig. 5 reveal corresponding changes when the surface orders. For $\Theta=3$ ML, feature *A* appears at 0.40 eV with an intensity comparable to feature *B*, and there is a pronounced Fermi edge. Feature *A* is much stronger for $\Theta=3.5$ ML, while feature *B* is suppressed. Feature *A* is so dominant at 4 ML that feature *B* cannot be identified and the IPES spectra are almost identical to those for [20 Å (~7.5 ML) Sb]/[*p*-type GaAs (110)] shown in Fig. 2. Energy-dependent IPES results demonstrate that the onset of the resonance at $\hbar\omega_p=15.9$ eV occurs at ~3.5 ML, as summarized in Fig. 6, where open triangles represent the (normalized) peak heights derived from feature *A* for $13.5 \leq E_i \leq 22.5$ eV. The shoulder at ~20 eV is due to the overlapping of feature *A* with the GaAs(110) excitonic feature at ~20.1 eV.^{25,26} In contrast, the peak heights for 3 ML of Sb exhibit no significant resonance (Fig. 6). At the onset of resonant IPES, feature *A* is not as sharp and symmetric as that seen for 4 ML. A broad high-energy shoulder with respect to E_F indicates that it has not thoroughly evolved from 0.40 to 0.30 eV because some areas associated with 3 ML are still not covered.

Overlayer morphology plays a very important role in determining the empty electronic structures of evolving thin films or interfaces. For ordered or epitaxial growth of Sb or Bi on GaAs(110), it might be possible to corre-

late structure changes with the various overlayer-derived surface-state bands. In an empirical tight-binding calculation for GaAs(110)-*p*(1×1)-Sb(1 ML), Mailhiot *et al.*¹¹ assumed that Sb formed zigzag chains backbonded to the chains of the Ga and As surface atoms of nearly unrelaxed GaAs(110).¹¹ This bridging-chain model gives the best agreement with recent (STM) images.¹⁴ Mailhiot *et al.* predicted two empty-surface-state bands, S_7 and S_8 , at 1.9 and 2.4 eV above the valence-band maximum (VBM) of GaAs(110) attributed to unoccupied antibonding combinations of the Sb-As and the Sb-Ga charge densities, respectively.¹¹ Experimentally, only one significant Sb-induced empty surface state, feature *B*, can be found at $E_F+2.0$ eV for GaAs(110)-*p*(1×1)-Sb(1 ML).²⁴ For $\Theta > 1$ ML, feature *A* gradually evolves with coverage (and annealing) and its energy spectra from feature *B* is 1.6 eV for (2 ML Sb)/[*p*-type GaAs(110)]. This difference is much larger than the predicted 0.5 eV separation between S_7 and S_8 , and it is hard to reconcile feature *A* as originating from S_7 . Analogous empty-electronic-state evolution has been found for Bi growth on GaAs(110), where only one Bi-derived surface-state band appears at $E_F+1.5$ eV for [*p*-type GaAs(110)]-*p*(1×1)-Bi(1 ML).¹⁹ For 2 ML Bi the second Bi-derived empty state, feature *A*, appears at $E_F+0.55$ eV. STM, LEED, and photoemission studies have confirmed that long-range-ordered patches of Bi adatoms grow atop the initial (1×1) monolayer for 2 ML Bi, even at 300 K.^{19,21} We conclude that feature *A* should be attributed to Sb-Sb or Bi-Bi interaction derived from long-range-ordered multilayers. Feature *B* can be associated with a surface-resonant state largely derived from Sb-Sb or Bi-Bi p_z - p_z π^* chain bonds.^{19,20}

The character of feature *A* depends strongly on its energy position and the structure of the thin film. As shown in Figs. 5 and 6, feature *A* exhibits strong resonant IPES at the constant photon energy $\hbar\omega_p=15.9$ eV as it shifts from ~0.4 eV at 3 ML to ~0.3 eV at 3.5 ML. It is noteworthy that the energy of this constant photon energy depends somewhat on the structural properties of the thin film and substrate, as pointed out recently by Drube and Himpsel.¹⁵ For instance, for (20 Å Sb)/InP(110) the energy is $\hbar\omega_p=16.4$ eV.

We have mentioned above that some of the six-pair modulation spots on the ring structure become visible for (~3.5 ML Sb)/GaAs(110), indicating that the hexagonal basal planes of the individual Sb crystallites begin to grow in two inequivalent quasihexagonal sites. LEED studies for this coverage suggest the coexistence of phases that construct a novel metastable structure (some phases may be in or out of registry with the substrate). For $1 < \Theta \leq 3$ ML, only those extra LEED spots adjacent to the integer-order spots can be seen (see Fig. 1), indicating that the Sb adatoms largely form ordered patches or domains that preserve (110) symmetry.²¹ These Sb patches or domains need not cover the entire first monolayer (thicker or thinner in some places), so that feature *B* from uncovered areas of the (1×1) first monolayer can still be seen in IPES of Figs. 4 and 5. With increasing coverages, the flattening of 3D clusters upon annealing might result in the growth of both the ordered domains

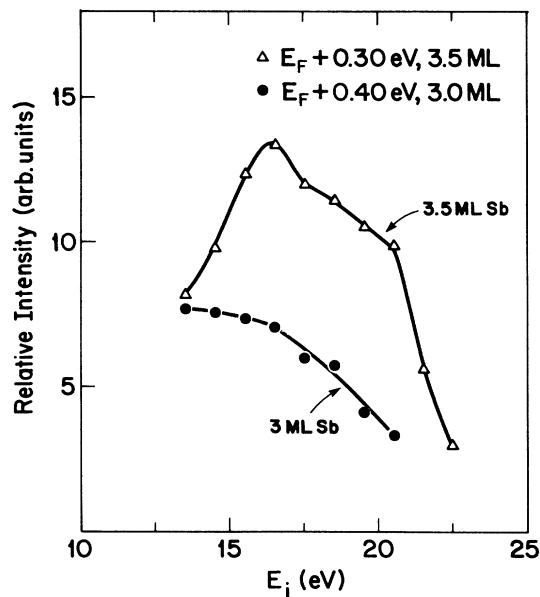


FIG. 6. Peak heights of feature *A* as a function of the incident energy E_i from spectra like those of Fig. 5. The solid circles were derived from feature *A* for 3 ML of Sb. The open triangles represent those derived from feature *A* for 3.5 ML. The onset of resonant IPES at the constant photon energy $\hbar\omega_p=15.9$ eV occurs at ~3.5 ML.

that preserve (110) symmetry and the hexagonal basal planes of individual Sb crystallites. Further suppression of feature *B* in IPES should depend on the distribution of these phases on the surface.

It is well known that the elongation of both the *a* and *b* axes of the crystal structure should be expected for single-phase growth of heteroepitaxial thin films. Instead, we find here that the *a* and *b* axes of crystalline Sb are constrained, based on analysis of the LEED ringlike structure. This suggests that the Sb crystallites grow between the ordered domains or in uncovered, low-coverage regions. A very schematic picture of this process is given in Fig. 7. Long-range ordering and flattening of 4 ML Sb overlayers on GaAs(110) are shown in the middle and bottom panels as a consequence of annealing of the as-grown disordered overlayer (top panel). Of course, we cannot rule out the possibility of local disorder, voids, and protrusions even after annealing (Fig. 7 is an oversimplified picture). The stresses on the Sb crystallites from the surrounding ordered domains gives rise to this unusual *a* and *b*-axis constraint of the Sb crystallites. This structure might not be stable for thick films, but it is for the appropriate thin films. It also makes it conceivable that Sb adatoms cover the (1×1) Sb monolayer continuously (but not necessarily uniformly). The full cover-

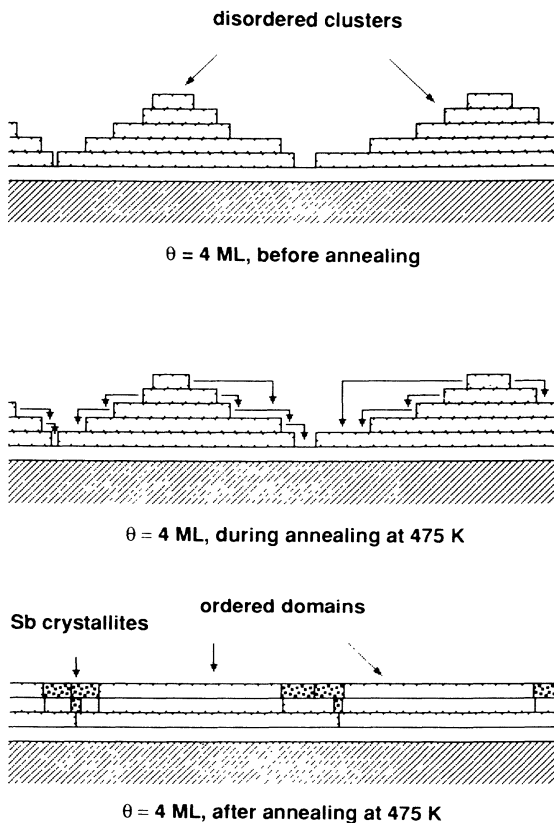


FIG. 7. Effects of the long-range ordering and flattening of 4 ML Sb overlayers on GaAs(110). Simplified pictures are given for deposition at 300 K, for annealing at 475 K, and after annealing at 475 K. We cannot rule out the possibility of the existence of local disorder, voids, and protrusions, even after annealing.

ing of the (1×1) Sb monolayer by Sb multilayers leads to the suppression of feature *B*, as observed in Fig. 5 for 4 ML, and the shift of feature *A* from 0.4 to 0.3 eV at 3.5 ML. [The mean-free-path effect alone is not enough to quench feature *B* between 3 and 4 ML, so that there must be some effect from the Sb-Sb interaction for long-range-ordered multilayers. We note that Demuth *et al.*²⁷ have found the formation of separated 2D (quasiperiodic) phases on the atomic scale for (5×5)-Cu/Si(111). It would be very interesting to obtain STM images for Sb thin films.]

The morphology of the Sb crystallites should depend on the initial growth conditions, the sizes or distributions of the ordered Sb domains, and the amount of Sb deposited. During growth of ~3.5 or 4 ML of Sb, the six pairs of the hexagonlike modulation spots dominate. This indicates that the Sb crystallites are not randomly rotated, but, instead, that two inequivalent quasi-hexagonal domains coexist. This is consistent with the very good match between the bulk nearest-neighbor distance (~4.02 Å) of Sb(0001) and the dimension (4.00 Å) of the unrelaxed GaAs(110) unit cell along [1 $\bar{1}$ 0]. Assuming a picture of two Sb atoms per unit cell for *p*(1×1)-Sb (1 ML),¹¹ a simple calculation suggests that two inequivalent half-hexagon sites (nearest-neighbor distance ~4.0 Å for an unrelaxed unit cell) are possible when the Sb-Sb bond length relaxes to the bulk value of 2.9 Å as coverage increases. In fact, we found the quasi-hexagonal unit cell to be somewhat constrained, as mentioned above, so that the critical thickness could be reduced to form this kind of the quasi-hexagon. [We have observed a similar but differently oriented quasi-hexagonal structure on another well-matched system, Bi/InP(110).] Since each half-hexagon needs only two (110) unit cells, Sb microcrystallites can form at low coverage. The result of these hexagonlike Sb domains parallel to (110) is also expected since the relative displacement perpendicular to the (110) surface, $\Delta_{1,\perp}$ between Sb (Ga) and Sb (As) in the *p*(1×1)-(1 ML) unit cell is less than 0.1 Å for *p*(1×1)-Sb(1 ML).^{5,8,11} Most of the relaxation toward the bulk value is within the (110) plane for the Sb-Sb bond length with further adatom deposition. For coverages near 20 Å Sb (~7.5 ML), the ringlike diffraction images are comparable to those modulation spots, since large amounts of Sb deposition result in randomly rotated growth of the hexagonal Sb basal planes.

We have also found that the resonance disappears if the surface is dominated by hexagonlike LEED patterns, corresponding to a complex lattice, consistent with results from Sb/InP(110).¹⁵ This happens at high nominal coverages (usually greater than ~10 ML) upon annealing above 475 K after 300 K deposition since coalescing of large clusters has occurred during growth.⁴ Drube *et al.*¹⁵ pointed out that stable, bulklike Sb thick films do not produce resonant IPES. They suggested that this is because the surface-matching condition of the dielectric function gives rise to a minimum emission of photons at the plasmon energy for bulklike, uniform single-phase thin films.¹⁶ The fact that no significant photon emission appears at $\hbar\omega_p = 15.9$ eV can also be understood because the photon momentum is not comparable to the electron

momentum for uniform, bulklike films. The coexistence of metastable, separated phases somehow provides various coupling conditions for the photon and electron momenta, and this depends on the distribution or separation of the Sb crystallites in the flat thin films, as shown in the bottom of Fig. 7.

CONCLUSIONS

We have used energy-dependent IPES and LEED to investigate long-range ordering and surface flattening of Sb multilayers grown on cleaved GaAs(110). Variations in the empty-electronic-state features have been determined as a function of coverage and annealing temperature. Two significant Sb-derived empty-state features, *A* and *B*, have been found during the evolution of ordered Sb multilayers. IPES studies reveal that feature *A* exhibits a strong resonant-photon emission at a constant photon energy of $\hbar\omega_p = 15.9$ eV when the film thickness exceeds ~ 3.5 ML. Feature *A* is associated with long-range ordering of Sb multilayers on GaAs(110), and it shifts from ~ 0.40 eV at 3 ML to ~ 0.30 eV at ~ 3.5 ML. Feature *B* at $E_F + 2.0$ eV for [*p*-type GaAs(110)]*p*(1×1)-Sb(1 ML) is suppressed when ordered Sb multilayers cover the initial first monolayer. The energy difference of ~ 1.6 eV at 2 ML Sb between features

A and *B* indicates that the Sb layer-layer interaction varies substantially from the initial *p*(1×1)-Sb(1 ML) structure to the ordered multilayers. In addition, the flattening and long-range ordering can also be seen from the appearance of a pronounced image-potential state at $E_F + 3.75$ eV.

LEED studies reveal that the resonant IPES behavior might be related to the growth of metastable ordered Sb(110) domains that coexist with quasihexagonal basal planes of individual Sb crystallites on GaAs(110). Phase separations might give rise to the coupling condition of photon and electron momenta at the plasmon energy. This indicates that the resonant IPES behavior is unique to the metastable thin film and explain why it cannot be observed for stable, bulklike Sb films. Hence, LEED and IPES results reveal that overlayer morphology plays a critical role in determining the empty electronic structures and resonances of thin films and interfaces.

ACKNOWLEDGMENTS

This work was supported by the U.S. National Science Foundation under Grant No. DMR-86-10837. We thank D. Poirier for technical assistance. Discussions with P. I. Cohen, T. Ohno, and Y.-N. Yang concerning LEED interpretation are gratefully acknowledged.

¹See, for example, H. Busch and M. Henzler, *Phys. Rev. B* **41**, 4891 (1990).

²P. Skeath, C. Y. Su, I. Lindau, and W. E. Spicer, *J. Vac. Sci. Technol.* **17**, 874 (1980).

³J. Carelli and A. Kahn, *Surf. Sci.* **116**, 380 (1982).

⁴R. Strümpfer and H. Lüth, *Surf. Sci.* **182**, 545 (1987).

⁵C. B. Duke, A. Paton, W. K. Ford, A. Kahn, and J. Carelli, *Phys. Rev. B* **26**, 803 (1982).

⁶M. Mattern-Klosson, R. Strüpler, and H. Lüth, *Phys. Rev. B* **33**, 2559 (1986).

⁷F. Schäffler, R. Ludeke, A. Taleb-Ibrahimi, G. Hughes, and D. Rieger, *J. Vac. Sci. Technol. B* **5**, 1048 (1987); *Phys. Rev. B* **36**, 1328 (1987).

⁸C. B. Duke, in *Surface Properties of Electronic Materials*, edited by D. A. King and D. P. Woodruff (Elsevier, Amsterdam, 1988), Chap. 3.

⁹P. Skeath, C. Y. Su, W. A. Harrison, I. Lindau, and W. E. Spicer, *Phys. Rev. B* **27**, 6274 (1983).

¹⁰C. M. Bertoni, C. Calandra, F. Mangli, and E. Molinari, *Phys. Rev. B* **27**, 1251 (1983).

¹¹C. Mailhot, C. B. Duke, and D. J. Chadi, *Phys. Rev. B* **31**, 2213 (1985).

¹²R. M. Feenstra and P. Mårtensson, *Phys. Rev. Lett.* **61**, 447 (1988).

¹³R. Cao, K. Miyano, I. Lindau, and W. E. Spicer, *Appl. Phys. Lett.* **53**, 137 (1988).

¹⁴P. Mårtensson and R. M. Feenstra, *Phys. Rev. B* **39**, 7744

(1989).

¹⁵W. Drube and F. J. Himpsel, *Phys. Rev. Lett.* **60**, 140 (1988).

¹⁶W. Drube, F. J. Himpsel, and P. I. Feibelman, *Phys. Rev. Lett.* **60**, 2070 (1988).

¹⁷Y. Gao, M. Grioni, B. Smandek, J. H. Weaver, and T. Tyrie, *J. Phys. E* **21**, 488 (1988).

¹⁸D. Straub, M. Skibowski, and F. J. Himpsel, *Phys. Rev. B* **32**, 5237 (1985).

¹⁹Yongjun Hu, T. J. Wagener, M. B. Jost, and J. H. Weaver, *Phys. Rev. B* **40**, 1146 (1989).

²⁰A. B. McLean and F. J. Himpsel, *Phys. Rev. B* **40**, 8425 (1989).

²¹A. B. McLean, R. M. Feenstra, A. Taleb-Ibrahimi, and R. Ludeke, *Phys. Rev. B* **39**, 12925 (1989); R. Ludeke, A. Taleb-Ibrahimi, R. M. Feenstra, and A. B. McLean, *J. Vac. Sci. Technol. B* **7**, 936 (1989).

²²M. A. Van Hove, W. H. Weinberg, and C.-M. Chan, in *Low-Energy Electron Diffraction* (Springer-Verlag, Berlin, 1986).

²³J. Donohue, in *Structures of the Elements* (Wiley, New York, 1982), p. 308.

²⁴W. Drube and F. J. Himpsel, *Phys. Rev. B* **37**, 855 (1988).

²⁵Yongjun Hu, T. J. Wagener, M. B. Jost, and J. H. Weaver, *Phys. Rev. B* **41**, 5817 (1990).

²⁶M. B. Jost, T. J. Wagener, Yongjun Hu, and J. H. Weaver, *Phys. Rev. B* **42**, 2937 (1990).

²⁷J. E. Demuth, U. K. Koehler, R. J. Hamers, and P. Kaplan, *Phys. Rev. Lett.* **62**, 641 (1989).